Monthly Notices
of the
ROYAL ASTRONOMICAL SOCIETY

MNRAS **438,** 2853–2863 (2014)
Advance Access publication 2014 January 13

doi:10.1093/mnras/stt2393

On the alignment of PNe and local magnetic field at the Galactic centre: magnetohydrodynamical numerical simulations

D. Falceta-Gonçalves[1,2]★ and H. Monteiro[3]

[1]*SUPA, School of Physics and Astronomy, University of St Andrews, North Haugh, St Andrews, Fife KY16 9SS, UK*
[2]*Escola de Artes, Ciências e Humanidades, Universidade de São Paulo, Rua Arlindo Bettio 1000, CEP 03828-000 São Paulo, Brazil*
[3]*Departamento de Física, Universidade Federal de Itajubá, Av. BPS 1303 - Pinheirinho, CEP 37500-903 Itajubá, Brazil*

Accepted 2013 December 10. Received 2013 December 9; in original form 2013 October 19

ABSTRACT

For the past decade, observations of the alignment of planetary nebulae (PNe) symmetries with respect to the Galactic disc have led to conflicting results. Recently, the first direct observational evidence for a real alignment between PNe and local interstellar magnetic fields in the central part of the Galaxy ($b < 5^\circ$) has been found. Motivated by the recent discovery, we studied the role of the interstellar magnetic field on the dynamical evolution of a planetary nebula by means of an analytical model and from 3D magnetohydrodynamical numerical simulations. In our models, the nebula is the result of a short-time event of mass ejection with its surrounding medium. The nebula asphericity is assumed to be due to an intrinsic shaping mechanism, dominated by the latitude-dependent asymptotic giant branch wind, and not the interstellar medium field. We test under what conditions typical ejecta would have their dynamics severely modified by an interstellar magnetic field. We found that uniform fields of $>100\,\mu$G are required in order to be dynamically dominant. This is found to occur only at later evolutionary stages, therefore, being unable to change the general morphology of the nebula. However, the symmetry axis of bipolar and elliptical nebulae end up aligned to the external field. This result can explain why different samples of PNe result in different conclusions regarding the alignment of PNe. Objects located at high Galactic latitudes, or at large radii, should present no preferential alignment with respect to the Galactic plane. PNe located at the Galactic centre and low latitudes would, on the other hand, be preferentially aligned to the disc. Finally, we present synthetic polarization maps of the nebulae to show that the polarization vectors, as well as the field lines at the expanding shell, are not uniform even in the strongly magnetized case, indicating that polarization maps of nebulae are not adequate in probing the orientation, or intensity, of the dominant external field.

Key words: hydrodynamics – methods: numerical – ISM: magnetic fields – planetary nebulae: general – Galaxy: bulge.

1 INTRODUCTION

Planetary nebulae are end products of the evolution of stars with masses below $8\,M_\odot$. The importance of these objects extends well beyond the physics that lead to the ejection of the outer layers of stars. Planetary nebulae (PNe) have also been key on understanding basic atomic processes, providing powerful tools to probe the physical and chemical characteristics of our Galaxy, on the understanding of the internal processes of low and intermediate mass stars, and others.

Since the work of Curtis (1918), many attempts have been made to classify PNe according to their morphology and correlate these with basic properties such as central star (CS) temperature, mass, position in the Galaxy and other parameters (see e.g. Khromov & Kohoutek 1968; Balick 1987; Balick & Preston 1987; Balick, Preston & Icke 1987; Icke, Preston & Balick 1989; Masson 1990; Schwarz 1994; Balick et al. 1997; Zhang & Kwok 1998; Stanghellini 1999; Manchado 2004). The myriad of different shapes observed can be basically classified in four major groups: round/spherical, ellipticals, bipolars and irregulars. It is not clear yet what process is dominant in shaping each morphology. A good summary of how morphological studies have been employed over the last half-decade to understand shaping mechanisms is given by Shaw (2012). Possibly more than one can operate in each object. Among the most plausible processes presented so far we have interacting outflows, magnetic fields, binarity and even the interaction of the ejecta with the interstellar medium (ISM).

★ E-mail: dfalceta@usp.br

The role of the ISM in shaping evolved PNe has been systematically investigated since the work of Gurzadyan (1969). A recent and extensive study on the classification of interacting PNe is presented by Ali et al. (2012). Wu et al. (2011) related the morphological features observed in several PNe with their relative motion with respect to the ISM. The dynamical interaction between the ISM and the PNe would occur basically in two ways: interaction with the interstellar magnetic field and due to a relative velocity between the central source and the surrounding medium. Analytical estimates (e.g. Smith 1976) and numerical simulations (e.g. Soker & Dgani 1997; Wareing, Zijlstra & O'Brien 2007) predict changes in nebular shape, as well as anisotropies in density and emission, when the central source is moving through the ISM. These are obviously unable to generally explain the different PN morphologies, but are quite successful in explaining the comet-like nebulae observed, as well as misplaced CSs with respect to the geometric centre of the nebula.

Regarding the magnetic fields, theoretical studies have been mostly focused on the early shaping of the nebulae, right after the envelope ejection (e.g. Heiligman 1980; Pascoli 1985; Stone & Norman 1992; García-Segura 1997; García-Segura et al. 1999; Balick & Frank 2002; Matt, Frank & Blackman 2006; Blackman 2008). The magnetic interaction of ISM magnetic fields and PNe has been just recently observed in Sh 2–216 (Ransom et al. 2008). These authors detected Faraday rotation along the PNe and were able to estimate the magnetic field intensity at the interaction region as $\sim 5 \pm 2\mu$G. The asymmetric radio emission revealed the compression of the ISM field by the nebula. These observations are in agreement, for instance, with the models of Soker & Dgani (1997). In this particular case though, there is little evidence for any role of the magnetic pressure in modifying the morphology of the nebula.

Apparent alignment of aspherical PNe with the interstellar magnetic field was first reported by Grinin & Zvereva (1968). Melnick & Harwit (1975) and Phillips (1997) claim to have obtained statistically relevant alignment between the major axis of elliptical and bipolar PNe with respect to the Galactic plane. Corradi, Aznar & Mampaso (1998) on the other hand studied a larger sample of objects getting no preferential alignment, and concluded that PNe are randomly oriented on the sky. These authors however did not compare the orientation of the PNe with estimates of the magnetic field orientation. Grinin & Zvereva (1968) showed that the correlation between the nebula axis of symmetry and the interstellar magnetic field orientation, probed by linear polarization, is much stronger than the correlation for the Galactic latitude. More recently, Weidmann & Díaz (2008) analysed over 400 objects all-sky and concluded that, as pointed by Corradi et al. (1998), PNe are in general not preferentially aligned to the Galactic plane. However, these authors found a correlation between the orientation of the major axis of some PNe and the Galactic plane for a small region of the sky, near the Galactic centre.

In a recent work, Rees & Zijlstra (2013) provided strong observational evidence for the alignment between PNe and the Galactic plane. They studied over 100 PNe at the Galactic centre with positive detection of alignment for bipolar nebulae. The statistics presented showed no relevant alignment for the other morphological types. These authors suggest that strong magnetic fields acted during the formation of the stars, driving a global alignment of stellar angular momenta with the large-scale magnetic field.

The considerations above lead naturally to the following questions:

(i) is it possible for the interstellar magnetic fields to tilt the PNe axis of symmetry, specially when these are initially misaligned with respect to the external field?

(ii) and, why does this effect seems to occur preferably at the Galactic centre?

Despite the achievements of the last few decades, no systematic study of the dynamical role of interstellar magnetic fields on the later evolution of PNe, with originally misaligned symmetries with respect to the ISM magnetic field, have been performed so far. This is exactly the problem we address in this paper.

In this work, we propose an alternative scenario to that proposed by Rees & Zijlstra (2013). We study the role of the interstellar magnetic field in changing, or distorting, the PNe large-scale morphologies. We assume that the initial shaping of the nebulae is done mainly by interacting winds, and magnetic fields have little effect in these initial stages. The effects of the external field appear at later stages, causing the original nebular asymmetry to be modified. We study if typical Galactic fields are able to distort the PN morphologies to account for the observed fraction. The manuscript is organized as follows. A simple analytic description of the dynamical evolution of a blast wave is provided in Section 2. The analytical estimates are then tested numerically, under a more detailed multidimensional study, as shown in Section 3, followed by the Conclusions.

2 DYNAMICS OF THE EXPANDING SHELL

The expansion of a spherical blast wave has been extensively studied theoretically in the past, in different contexts from acoustic blast waves in the atmosphere (Taylor 1950), stellar winds (Weaver et al. 1977) to SN remnants (Woltjer 1972; Melioli et. al. 2006) and in the magnetized case (e.g. Heiligman 1980; Stone & Norman 1992; Soker & Dgani 1997; Leão et. al. 2009).

There is no consensus yet on the detailed physics that triggers the post-AGB superwinds. Current stellar evolution models study the role of angular momentum, pulsations and magnetic fields on them. Despite model uncertainties it is clear that the process of envelope ejection is very fast, and must occur at very short transition time-scales ($\tau_{\rm trans} \ll 10^3$ yr) compared to the lifetimes of observed PNe ($t \sim 10^4$ yr) (see Van Winckel 2003, for a review). Besides, assuming a typical expansion velocity of $\sim$100 km s^{-1}, the nebula is mass/energy loaded up to a length-scale $l < 10^{-3}$ pc. Both time- and length-scales for the superwind to load the nebula are very small compared to those we are interested in this work, and we may then assume the energy injection as quasi-instantaneous. In this case, we can model the expansion of the PN over the ISM as a single blast.

For the sake of simplicity, let us consider a planetary nebula as the result of a total mass ejection M_0, occurring in a short time event (shorter than the typical expansion time-scales) with initial energy E_0. After the burst the material adiabatically expands over the surrounding ambient medium. The expansion occurs initially due to the work done by the internal pressure over the ambient cold gas, in which pressure is negligible compared to the total energy density of the blast wave. The radius of the expanding shell $R_{\rm s}$ is obtained as a function of time by assuming that energy is conserved as

$$R_{\rm s}^{\rm adi}(t) \sim \left(\frac{E_0}{\rho_{\rm ISM}}\right)^{1/5} t^{2/5}, \qquad (1)$$

where $\rho_{\rm ISM}$ represents the mass density of the ISM. The velocity is readily obtained as $V_{\rm s}^{\rm adi}(t) \sim \left(\frac{E_0}{\rho_{\rm ISM}}\right)^{1/5} t^{-3/5}$.

The adiabatic phase lasts until the radiative losses become relevant at the shock, i.e. when $\int \dot{E}_{\rm rad} {\rm d}t' \sim E(t)$. The determination of the transition time ($t = \tau_{\rm rad}$), between the adiabatic and radiative

phases, depends on the radiative cooling curve assumed. For typical solar abundances (Weaver et al. 1977):

$$\int \dot{E}_{\rm rad} {\rm d}t' \simeq 0.32 n_{\rm ISM}^{9/5} E_0^{1/5} t^{17/5}, \tag{2}$$

which gives a transition time-scale of

$$\tau_{\rm rad} \sim E_0^{4/17} n_{\rm ISM}^{-9/5}. \tag{3}$$

For $E_0 \sim 10^{45}$ erg and $n_{\rm ISM} \sim 1\,{\rm cm}^{-3}$, one obtains $\tau_{\rm rad} \sim 300$ yr, which is short compared to the typical PNe lifetimes $\sim 10^4$ yr. If $R_{\rm rad}$ and $V_{\rm s}$ correspond to the shell radius and velocity at the transition time, the values given above result in $R_{\rm rad} \sim 0.04$ pc and $V_{\rm s,rad} \sim 200\,{\rm km\,s}^{-1}$.

At $t > \tau_{\rm rad}$, momentum conservation can be used instead, i.e. $R_{\rm s}^3 V_{\rm s} \rho_{\rm ISM} \simeq$ const., which results in

$$R_{\rm s} \simeq R_{\rm rad} \left(\frac{8}{5} \frac{t}{\tau_{\rm rad}} - \frac{3}{5} \right)^{\frac{1}{4}} \tag{4}$$

and

$$V_{\rm s} \simeq V_{\rm rad} \left(\frac{8}{5} \frac{t}{\tau_{\rm rad}} - \frac{3}{5} \right)^{-\frac{3}{4}}. \tag{5}$$

The total mass of interstellar gas that is swept up and accumulates at the expanding shell is approximately given by $M_{\rm s} \simeq \rho_{\rm ISM} R_{\rm s}^3 (4\pi/3)$. Therefore, the kinetic energy density, i.e. the ram pressure, may be estimated as

$$p_{\rm ram} \simeq \rho_{\rm ISM} V_{\rm s}^2 \frac{R_{\rm s}^3}{\left[R_{\rm s}^3 - (R_{\rm s} - \Delta)^3 \right]} \tag{6}$$

being Δ the thickness of the outer shock region, defined as the region between the contact discontinuity and the shock surface between the ISM and the expanding shell. Since the radiative losses are assumed to be very efficient $\Delta \ll R_{\rm s}$ and $p_{\rm ram} \sim \rho_{\rm ISM} V_{\rm s}^2 (1 - 3\Delta)^{-1}$. The shell ceases its expansion once the ram pressure is reduced, and balanced with the ambient pressure.

2.1 Magnetic fields

Once the ISM is considered magnetized not only the ambient gas is dragged and accumulated at the expanding shell, but also the magnetic field lines. The result is an increase in the total pressure at the outer shock, and a reduction on the expansion of the nebula compared to the pure hydrodynamical case.

The process is understood as follows. In the hydrodynamical case, most of the kinetic energy of the shock wave is transferred to the ambient gas as thermal energy. The remaining energy is kept as kinetic for the shocked gas to keep expanding. In the magneto-hydrodynamical (MHD) case, part of the energy of the shock wave that would be transformed into thermal energy is actually converted into magnetic one. This occurs once the magnetic field lines are compressed together with the ambient gas. The magnetic pressure increases in the outer shock region and, as a consequence, the temperature of the shock gas is lower compared to the hydrodynamical case. The magnetic pressure acts in the direction perpendicular to the field lines, i.e. for $\boldsymbol{V}_{\rm s} \perp \boldsymbol{B}_0$. There is free expansion along the field lines.

Let us reconsider the problem of a spherical blast wave propagating over a homogeneous ambient medium, but now threaded by a uniform magnetic field B_0. Also, let us consider that the ISM magnetic field is weak compared to the kinetic energy density of the blast. This assumption allows us to treat the expansion as isotropic and the results of equations (3)– (5) remain valid. Once the shell reaches a radius $R_{\rm s}$, at $t > \tau_{\rm rad}$, it has also dragged interstellar magnetic field lines into the outer shock layer. The magnetic pressure is given by

$$p_{\rm mag}(\theta) \simeq \frac{B_0^2}{8\pi} |\sin\theta| \frac{R_{\rm s}^3}{\left[R_{\rm s}^3 - (R_{\rm s} - \Delta)^3 \right]}, \tag{7}$$

where θ is the angle between $\boldsymbol{V}_{\rm s}$ and $\boldsymbol{B}_0$, at a given position over the shell. The magnetic pressure is therefore not isotropic at the outer shock region. The magnetic energy is accumulated most at the regions where expansion occurred perpendicular to the ambient field lines.

The free expansion of the nebula will cease at different time-scaling depending on θ. The expansion will occur as described for the unmagnetized case on the direction parallel to the field lines. On the perpendicular direction, the stall occurs earlier, once $p_{\rm ram} \sim p_{\rm mag}(\theta = \pi/2)$.

The ratio between the kinetic and magnetic pressure within the outer shock region, for $t \gg \tau_{\rm rad}$, is

$$\beta \equiv \frac{p_{\rm ram}}{p_{\rm mag}(\theta = \pi/2)} \approx \frac{8\pi \rho_{\rm ISM} V_{\rm rad}^2}{\sin\theta B_0^2} \left(\frac{8}{5} \frac{t}{\tau_{\rm rad}} \right)^{-5/4}. \tag{8}$$

Initially, considering typical ISM and PN properties, one expects $\beta(\theta) \gg 1$ everywhere in the nebula. The transition from kinetic to magnetically dominated dynamics (equipartition) occurs when $\beta \simeq 1$, i.e. when

$$\tau_{\rm equip} \approx 2.5 \times 10^{-2} \left(\frac{E_0}{10^{45}{\rm erg}} \right)^{4/17} \left(\frac{V_{\rm s,rad}}{200{\rm km\ s}^{-1}} \right)^{8/5} \times \left(\frac{n_{\rm ISM}}{1{\rm cm}^{-3}} \right)^{23/85} \sin\theta^{-4/5} B_0^{-8/5}\ {\rm yr}. \tag{9}$$

From the equation above, for a typical local ISM magnetic field of $B_0 = 2$–$5\,\mu$G one obtains $\tau_{\rm equip} \simeq 10^7$ yr, for $\theta = \pi/2$. This time-scale is too large compared to the typical ages of PNe, $\sim 10^4$ yr, and, in this case, the magnetic fields would have little effect on the dynamics of the nebula. The time-scale $\tau_{\rm equip}$ is shown in Fig. 1 as a

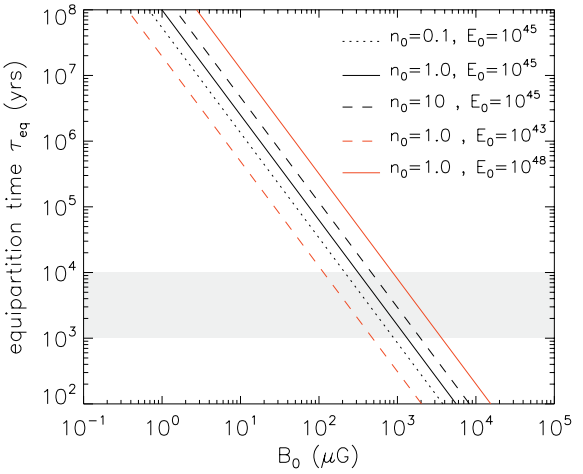

Figure 1. The equipartition time-scale $\tau_{\rm equip}$ as a function of the ambient magnetic field B_0. The lines correspond to different sets of initial energy input E_0 and interstellar density $n_{\rm ISM}$. Black lines were obtained for $E_0 = 10^{45}$ erg with $n_{\rm ISM} = 0.1\,{\rm cm}^{-3}$ (dotted), $1\,{\rm cm}^{-3}$ (solid) and $10\,{\rm cm}^{-3}$ (dashed). Red lines were obtained for $n_{\rm ISM} = 0.1\,{\rm cm}^{-3}$ with $E_0 = 10^{48}$ erg (solid) and 10^{42} erg (dashed). The grey area corresponds to $\tau_{\rm equip} < 10^4$ yr, i.e. shorter than the typical ages of planetary nebulae.

function of B_0 for different interstellar gas densities. The grey area corresponds to the typical observed range of ages. We infer from this simple model that the dynamics of a PN will be modified by the ISM magnetic fields for $B_0 > 100\,\mu$G.

Note that for the estimate above we have disregarded the stellar magnetic field. The reason is that surface magnetic fields in the range of $B_* \sim 10^{-3}$–10^{-2} G result in magnetic pressures of 10^{-8}–$10^{-6}\,\mathrm{erg\,cm^{-3}}$, many orders of magnitude smaller than the ram pressure of the wind ($>10^{-2}\,\mathrm{erg\,cm^{-3}}$). If we consider the magnetic field intensity to decay with r^{-2}, as for a monopolar configuration in a super-Alfvénic wind, the influence of the magnetic field of the star is even weaker at larger distances. Except for extreme cases (with $B_* \gg 1$ G), the stellar magnetic field is irrelevant for the late dynamics of the nebula, and may be neglected.

Obviously, the magnetized case is essentially anisotropic and a more detailed and multidimensional analysis is needed for a complete understanding of the problem. Also, the influence of the magnetic field during the adiabatic phase was not taken into account, as well as other features such as the generation and propagation of magnetosonic and Alfvén waves. In this sense, we provide a numerical analysis of the problem in the following section with the main goal of testing the validity of the previous estimates.

3 MHD NUMERICAL SIMULATIONS OF PN EJECTA

During their asymptotic giant branch (AGB and pre-PN phases) intermediate mass stars are supposed to preset strong winds. Depending on stellar rotation or other mechanisms, such as binarity or large-scale magnetic fields, the winds may present latitudinal dependence, which result in a circunstellar matter density distribution that is also aspherical. The terminal phases of envelope ejection, at the end of the pre-PN phase, is expected to interact with the anisotropic medium that will change its expansion velocities. The result is a global morphology that can vary from a spherical shell, to elliptical and bipolar ones. The so-called 'interacting winds' model has been quite successful in explaining global morphologies of PNe (Icke, Balick & Frank 1992).

A proper physical description of the formation of a PN would be the result of a complete modelling of the stellar winds during the AGB and post-AGB phases, together with a comprehensive study of the internal conditions during the formation of the white dwarf and how it decouples from the envelope. Such details may be important but cannot be treated properly in our models. We must simplify the initial setup of the problem and focus simply on the dynamical evolution of the nebula as it interacts with the surrounding magnetized ISM.

AGB stars present massive stellar winds, with mass-loss rates of $\dot{M} \sim 10^{-9}$–$10^{-5}\,\mathrm{M_\odot\,yr^{-1}}$, and terminal velocities of $u_\infty \sim 10$–$100\,\mathrm{km\,s^{-1}}$, for periods as long as 100 000 yr (Falceta-Gonçalves & Jatenco-Pereira 2002; Vidotto, Falceta-Gonçalves & Jatenco-Pereira 2006; Falceta-Gonçalves, Vidotto & Jatenco-Pereira 2006). Considering a typical low density ($n \leq 1\,\mathrm{cm^{-3}}$) and weakly magnetized ISM ($B \sim 1$–$5\,\mu$G), such a wind would carve the interstellar gas to create an asteropause as large as ∼0.1–1 pc. Large ISM turbulent/thermal pressure, or strong magnetic fields, would naturally reduce this estimate. In the case of $B > 100\,\mu$G, as discussed in the previous section, the asteropause would be limited to radii <0.01 pc. The wind-ISM coupling results in two distinct regions for the expanding PN. One is defined from the star up to few thousands of au, where the ISM influence is negligible, and the stellar ejecta interact only with the extended envelope, i.e. the previously ejected stellar winds. The second region is defined above the mentioned region, from which the ISM magnetic pressure dominates the dynamics of the nebula. From this scenario, it is straightforward to assume the general morphology of the PNe (round, elliptical or bipolar) to be determined by the interaction of the post-AGB superwind with the earlier aspherical AGB wind, with little effect of the ISM magnetic field. However, once the nebula reaches the asteropause it should interact with an unperturbed external ISM.

As mentioned earlier, there is no consensus about what mechanism dominates the shaping of PNe. For this work in particular, the actual shaping mechanism is irrelevant since we focus on the interaction of an already shaped nebula with the surrounding ISM. A straightforward way of generating axisymmetric nebulae for our models is to use the interacting winds method. The post-AGB superwind is driven and expands over a preset gas distribution which is latitude dependent. The enhanced density at the equatorial plane results in slower expansion velocities on those directions. The end product is a latitude-dependent expanding nebula. Few prescriptions for the preset density distribution were given (e.g. Kahn & West 1985; Icke et al. 1989; Mellema, Eulderink & Icke 1991), though none of these based on self-consistently driven wind models. For the sake of simplicity, we use the same setup as in Monteiro & Falceta-Gonçalves (2011). In such model, the preset ambient gas distribution – determined during the stellar AGB phase – should follow the distribution (as used by Icke et al. 1989; Mellema et al. 1991):

$$\rho_{\mathrm{amb}} = \frac{\rho_0}{A(\theta)}\left(\frac{r_0}{r}\right)^2, \tag{10}$$

where

$$A(\theta) = 1 - \alpha\left(\frac{e^{\delta\cos 2\theta - \delta} - 1}{e^{2\delta} - 1}\right), \tag{11}$$

being the parameter α related to the density ratio at the polar and equatorial directions, and δ the steepness of the density profile with the latitude.

The above equations represent an initial setup for the matter distribution, together with the implementation of an energy source (blast wave) at the stellar location, and the external magnetic field. The interaction of the blast wave with the preset density distribution, and later with the external magnetic field, will determine the final global morphology of the nebula.

3.1 Governing equations and numerical setup

The dynamical evolution of the blast wave, and of the magnetized ISM, is governed by the MHD, which can be written in the conservative form:

$$\partial_t \boldsymbol{U} + \nabla\cdot\boldsymbol{F}(\boldsymbol{U}) = f(\boldsymbol{U}), \tag{12}$$

where $f(\boldsymbol{U})$ is the source term, $\boldsymbol{U}$ is the vector of conserved variables:

$$\boldsymbol{U} = \left(\rho, \rho\boldsymbol{V}, \left(\frac{1}{\gamma-1}p + \frac{1}{2}\rho v^2 + \frac{B^2}{2}\right), \boldsymbol{B}\right)^T \tag{13}$$

and $\boldsymbol{F}$ is the flux tensor:

$$\boldsymbol{F} = \left(\rho\boldsymbol{V}, \rho\boldsymbol{V} + p_{\mathrm{tot}}\boldsymbol{I} - \boldsymbol{B}\boldsymbol{B} <, \left(\frac{\gamma}{\gamma-1}p + \frac{1}{2}\rho v^2\right)\boldsymbol{V} - \boldsymbol{B}(\boldsymbol{B}\boldsymbol{V}), \boldsymbol{V}\boldsymbol{B} - \boldsymbol{B}\boldsymbol{V}\right)^T, \tag{14}$$

Table 1. Parameters used in each simulation.

Model	α	Global morphology	B_0(μG)	θ	Dimensions	Resolution (pixels)
SPH1	0.0	spherical	5	45°	2.5D	2048 × 1024
SPH2	0.0	spherical	50	45°	2.5D	2048 × 1024
SPH3	0.0	spherical	500	45°	2.5D	2048 × 1024
SPH4	0.20	spherical	5	45°	2.5D	2048 × 1024
SPH5	0.20	spherical	50	45°	2.5D	2048 × 1024
SPH6	0.20	spherical	500	45°	2.5D	2048 × 1024
SPH7	0.20	spherical	5	45°	3D	512 × 256 × 256
SPH8	0.20	spherical	500	45°	3D	512 × 256 × 256
ELI1	0.60	elliptical	5	45°	2.5D	2048 × 1024
ELI2	0.60	elliptical	50	45°	2.5D	2048 × 1024
ELI3	0.60	elliptical	500	45°	2.5D	2048 × 1024
ELI4	0.60	elliptical	5	45°	3D	512 × 256 × 256
ELI5	0.60	elliptical	500	45°	3D	512 × 256 × 256
BIP1	0.80	bipolar	5	45°	2.5D	2048 × 1024
BIP2	0.80	bipolar	50	45°	2.5D	2048 × 1024
BIP3	0.80	bipolar	500	45°	2.5D	2048 × 1024
BIP4	0.95	bipolar	5	45°	2.5D	2048 × 1024
BIP5	0.95	bipolar	50	45°	2.5D	2048 × 1024
BIP6	0.95	bipolar	500	45°	2.5D	2048 × 1024
BIP7	0.95	bipolar	500	30°	2.5D	2048 × 1024
BIP8	0.95	bipolar	500	60°	2.5D	2048 × 1024
BIP9	0.95	bipolar	5	45°	3D	512 × 256 × 256
BIP10	0.95	bipolar	500	45°	3D	512 × 256 × 256

where ρ is the gas mass density, $\boldsymbol{V}$ the fluid velocity, $\boldsymbol{B}$ the magnetic field, p the thermal pressure, $p_{\rm tot} = p + B^2/8\pi$ $p_{\rm tot} = p + p_{\rm mag}$ the total pressure, and γ the adiabatic polytropic index, and f corresponds to source terms for the given conserved variable U. The set of equations is closed by calculating the radiative cooling as source term for the energy equation, as follows:

$$\frac{\partial p}{\partial t} = \frac{1}{(1-\gamma)} n^2 \Lambda(T), \tag{15}$$

where n is the number density and $\Lambda(T)$ is the cooling function, which is obtained through an interpolation method of the electron cooling efficiency table for an optically thin gas (Gnat & Sternberg 2007).

In the simulations, the above set of equations was solved using the GODUNOV code,[1] which has been extensively tested and used in many astrophysical problems (e.g. Falceta-Gonçalves et al. 2010a, 2010b; Falceta-Gonçalves, Lazarian & Houde 2010c; Kowal & Lazarian 2010; Falceta-Gonçalves & Lazarian 2011; Kowal, de Gouveia Dal Pino & Lazarian 2011b; Kowal, Falceta-Gonçalves & Lazarian 2011a; Kowal, de Gouveia Dal Pino & Lazarian 2012; Poidevin et al. 2013; Ruiz et al. 2013). The spatial reconstruction is obtained by a fifth-order monotonicity-preserving method (He et al. 2011), with approximate Harten-Lax-van Leer-Contact Riemann solver (Mignone & Bodo 2006). The time integration is performed with the use of a third-order four-stage explicit optimal Strong Stability Preserving Runge–Kutta [SSPRK(4,3)] method (Ruuth 2006). For the magnetic field, we make use of a hyperbolic divergence cleaning approach (Dedner et al. 2002).

Initially, we performed a number of 2.5-dimensional models with high resolution in order to obtain the general trends in the observed morphology. The computational domain is defined as a uniformly distributed grid, in Cartesian coordinates, with 2048 × 1024 cells along x and y directions, respectively, corresponding to sizes of 1 and 0.5 in code units. Each code unit in length corresponds to 0.2 pc, which results in a spatial resolution of approximately 9.6×10^{-5} pc per pixel. Following, we selected few models, as described in Table 1, to run in full three-dimensional simulations. For these, due to computational resources, the numerical resolution is set as 512 × 256 × 256 cells along x-, y- and z-axis.

The ambient density is initially set as in equations (10) and (11). For the sake of simplicity in running the models, we fixed $\delta = 1.0$ since its role on the global shape of the nebulae is less than that of $\alpha = 1.0$. The blast is initiated by a total energy injection of 10^{45} erg inside a sphere of radius $r_0 = 0.02$ c.u., as in the simulations performed by (Monteiro & Falceta-Gonçalves 2011). The ambient medium magnetic field is assumed to be initially uniform, set as $\boldsymbol{B}_0$, with a given angle θ with respect to the axis of symmetry of the nebula. The simulations are performed for a range of intensities B_0 and inclinations θ of the ambient magnetic field with respect to the symmetry axis of the nebula.

3.2 PN morphology and dynamics

As a general result from the simulations we found that the global morphologies obtained are basically independent on the magnetic field intensity, at least for the values of B_0 set in the simulations. It is clear from Fig. 1 that the external magnetic field would only modify the global morphology of the blast wave for $B_0 > 1$mG. Therefore, the main parameter for determining the shape of the nebula is α.

The main role of the magnetic field in our models is to change the expansion velocity of the blast wave at a larger distance from the source. In this sense, the morphology is not greatly changed – as we show below – but the axis of symmetry of the nebula is tilted, depending on the magnetic field intensity. We start the morphological and kinematic analysis using the bipolar models as basic reference, since these have been used recently by Rees & Zijlstra (2013) to probe the magnetic field in the Galactic centre. In Fig. 2, we show the density distributions of models BIP4, BIP5 and BIP6. In all three cases, the general morphology observed is clearly

[1] http://amuncode.org

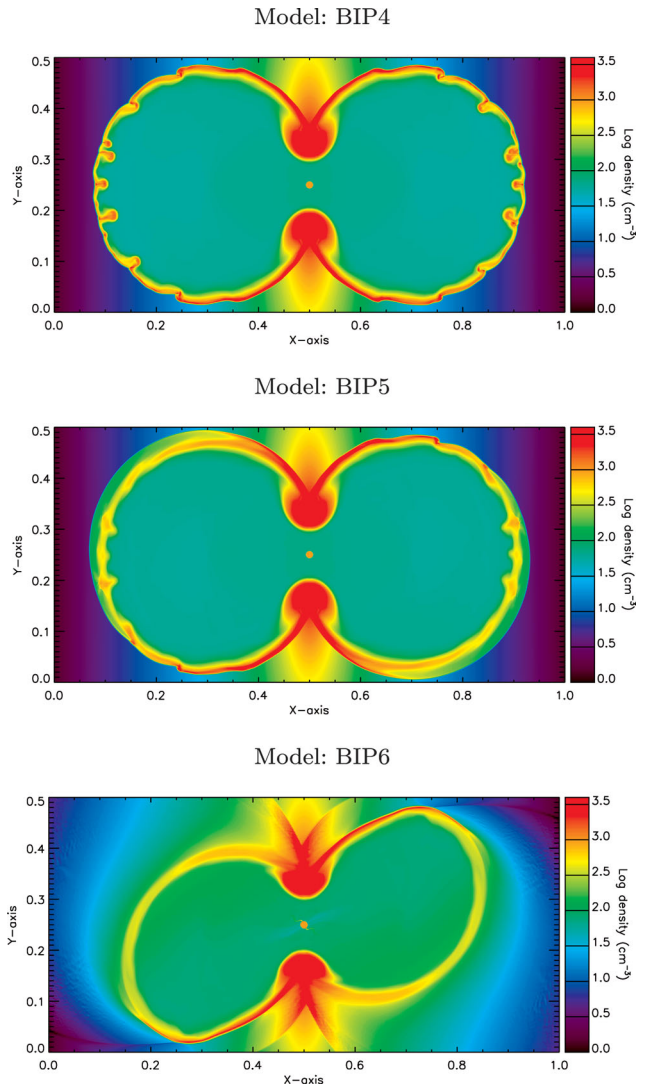

Figure 2. Density maps in logarithmic scale for models with $\alpha = 0.95$ and $\delta = 0.1$. The ambient magnetic field intensity is initially uniformly set, from top to bottom, as $B_0 = 5$, 50 and 500 μG, respectively.

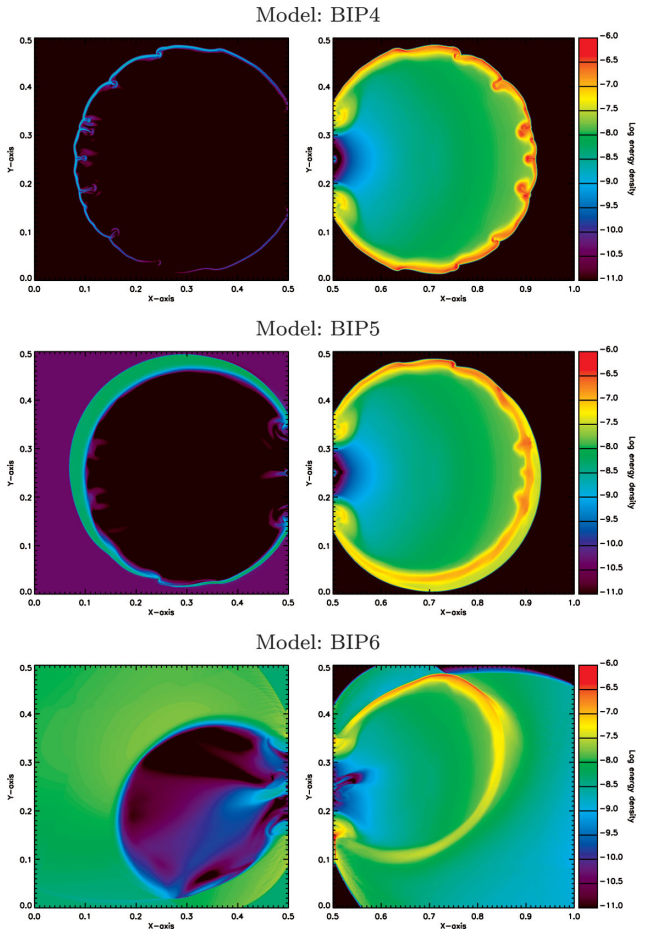

Figure 3. Magnetic energy density map (left) and kinetic energy density map (right) for models with $\alpha = 0.95$ and $\delta = 0.1$. Both maps are in logarithmic scale. The ambient magnetic field intensity is initially uniformly set, from top to bottom, as $B_0 = 5$, 50 and 500 μG, respectively.

bipolar with little changes in the nebular shapes for increasing magnetic field intensity, except for the slightly narrower lobes found for $B_0 = 500\,\mu$G. The main difference occurs on the orientation of the lobes. For $B_0 = 5\,\mu$G, the axis of symmetry is kept exactly as initially set by the density distribution. Small differences are perceived for $B_0 = 50\,\mu$G, where the nebula present an anisotropy in the density distribution. However its axis of symmetry is not changed. For $B_0 = 500\,\mu$G the density distribution of the nebula is greatly changed, with reduced importance of the local instabilities that create the knots and clumps. The magnetic tension plays a role as stabilizing source. At the same time, the expansion is prevented at the directions perpendicular to the field lines. The result is the tilted axis of symmetry of the nebula, in rough agreement with the orientation of the external field, i.e. 45° with respect to the initial axis of symmetry of the preset ambient density distribution.

In agreement with the dynamical evolution described from an analytical point of view in Section 2, the nebula will be tilted by the magnetic field if the kinetic pressure of shell is small, compared to the magnetic energy density. This behaviour is illustrated quantitatively in Fig. 3, where the kinetic and magnetic energy densities are shown for the bipolar nebulae models BIP4, BIP5 and BIP6. These maps present the same colour table for both physical quantities, and it is possible to directly compare the colours in both maps in order to visualize where equipartition is obtained. For $B_0 = 5\,\mu$G (top) the magnetic energy density (left), $\epsilon_B \sim 10^{-10}$–10^{-9} erg cm^{-3}, is clearly smaller than the kinetic energy density (right), $\epsilon_{\rm kin} \sim 10^{-7}$–$10^{-6}$ erg cm^{-3}. The magnetic field intensity is enhanced at the shell though, forming a narrow magnetized region due to the pile-up effect that occurs as the nebula drags the ambient field lines that accumulate as it expands.

The local increase of the magnetic pressure is more clearly seen in the model with $B_0 = 50\,\mu$G (middle). Here, two different regions are seen in the nebula. One, denser, is dominated by the kinetic energy and is less affected by the external field. Surrounding this dense shell there is a smooth region where both energies are closely in equipartition. This region is broadened due to larger velocities of the perturbations – understood here as Alfvén and fast magnetosonic modes – generated by the compression of the ambient gas. Note that this broader region is asymmetric with respect to the axis of symmetry of the nebula, being broader in the direction perpendicular to the external magnetic field. This effect does not occur for model BIP4 because the expansion velocity of the shell is larger than those of the Alfvén modes.

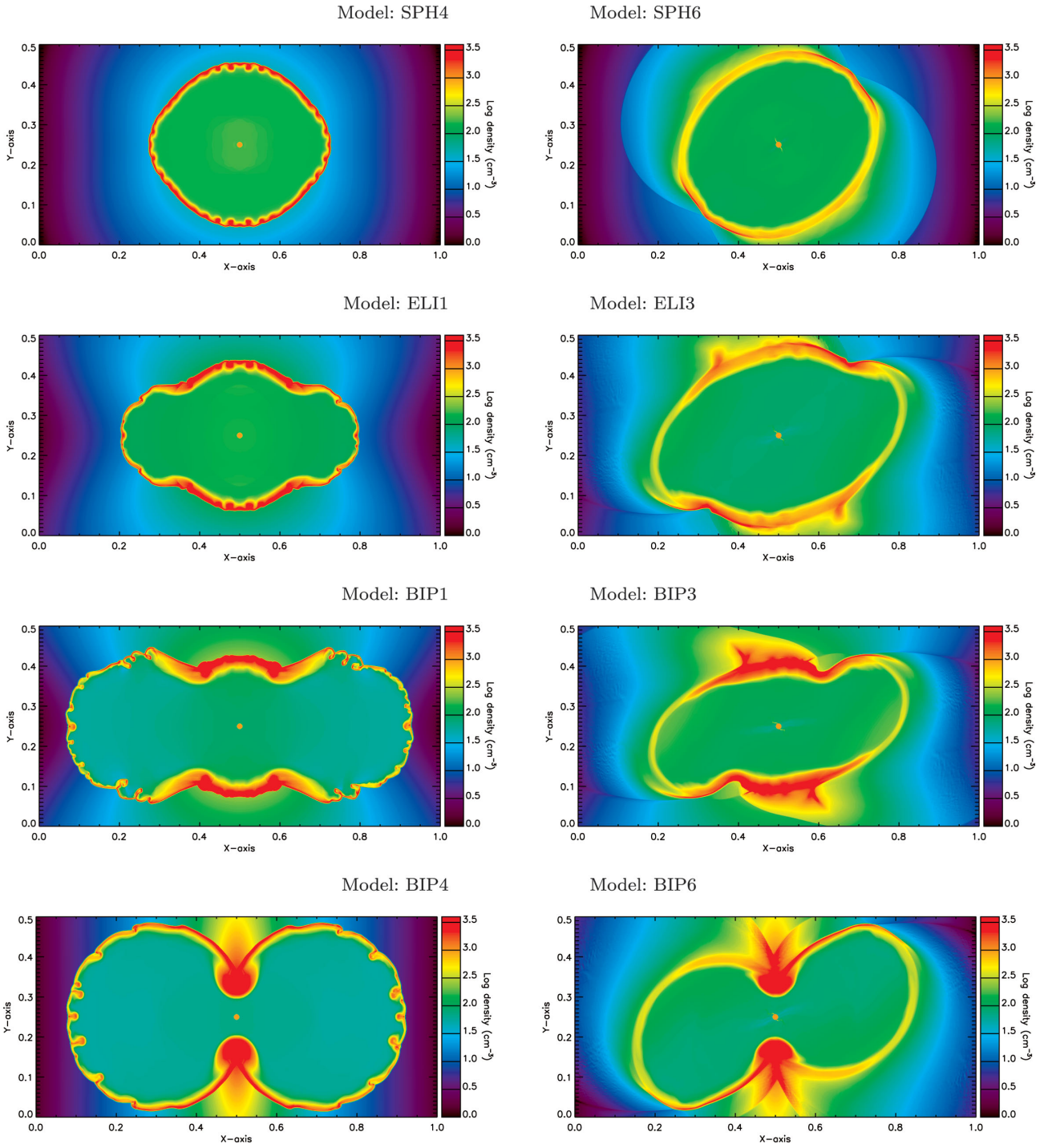

Figure 4. Density maps in logarithmic scale for models with, from top to bottom, $\alpha = 0.2$, 0.6, 0.8 and 0.95. The ambient magnetic field intensity is initially uniformly set as $B_0 = 5$ μG (left) and 500 μG (right).

Finally, for $B_0 = 500$ μG (bottom), the magnetic energy density is large during most of the simulation and the expansion of the nebula is possible to occur on the direction parallel to the external field lines (notably the only regions where $\epsilon_{\rm kin}$ is substantially larger than ϵ_B). It is interesting to note here that the blast generates magnetosonic waves that propagate fast on the opposite direction, i.e. perpendicular to the ambient magnetic field. Such waves have little effect in generating density enhancements but could be identified as source of local turbulence, or heating, as they non-linearly decay.

All other models run present the same trend as has been discussed above, i.e. all models with $B_0 = 5$ μG showed no changes in morphology due to the external magnetic fields, while the models with $B_0 = 500$ μG presented tilted axis of symmetries aligned to the field lines. We chose models that represent each of the morphological groups to be shown in Fig. 4. All models, except SPH6,

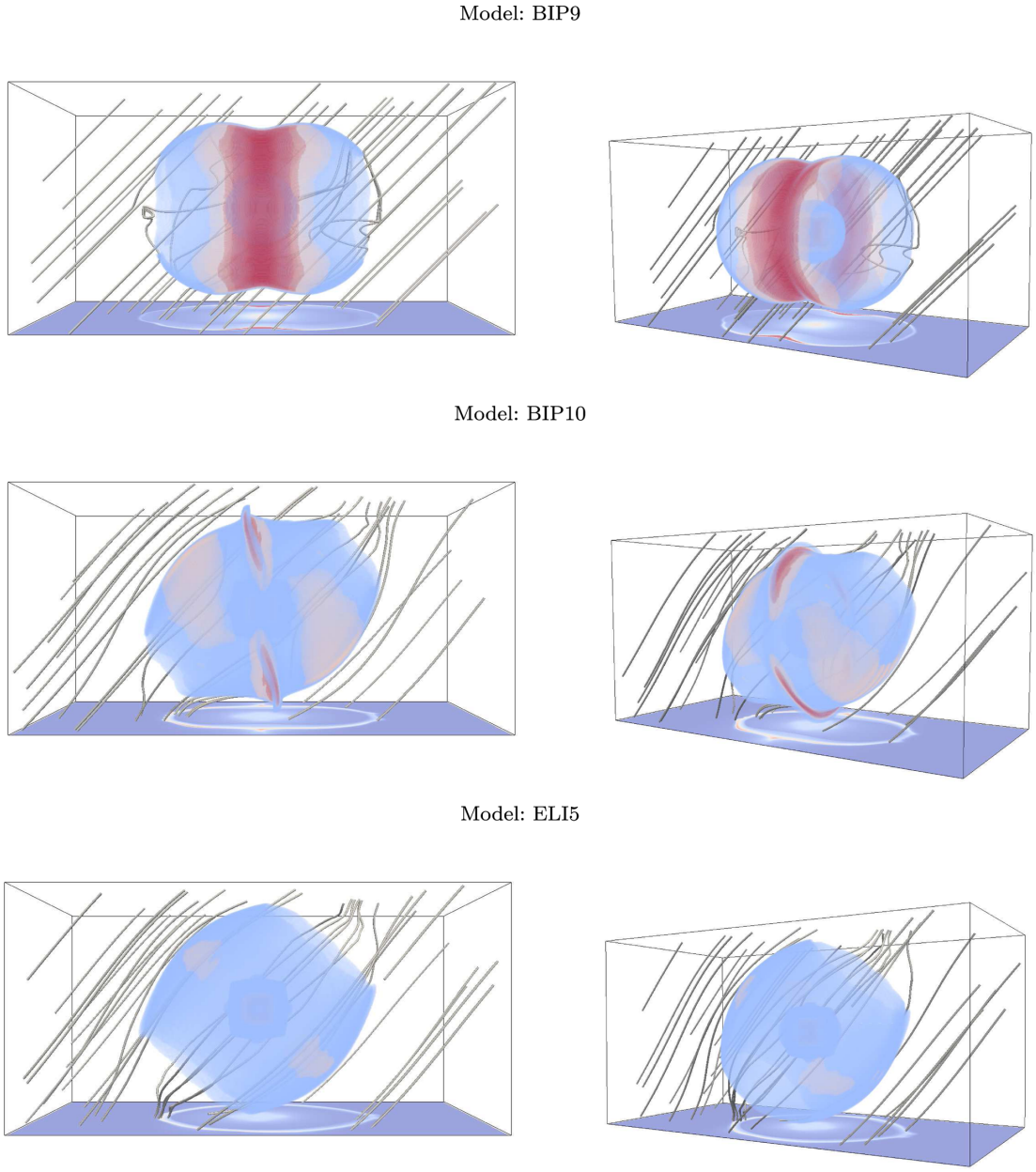

Figure 5. Three-dimensional visualization of the shell morphology and its relationship with the external ISM magnetic field lines for the two models with $\alpha = 0.95$, being $B_0 = 5\ \mu$G (top) and $B_0 = 0.5$mG (middle). The bottom images represent the projections obtained for model with $\alpha = 0.6$ (elliptical) and $B_0 = 0.5$mG. The visualizations were obtained for two LOS, the first along z-axis and the second with an angle of 30°.

which is supposed to be spherical, present asymmetries aligned to the external field for $B_0 = 500\ \mu$G.

The three-dimensional structure of the nebula is exactly as shown in the two-dimensional maps. In order to provide the reader a more realistic visualization of the nebula and the environment field lines, we provide in Fig. 5 the projections of the density from models BIP9 and BIP10. The figures are simply a volumetric projection of the density distribution along a given line of sight. Here, we illustrate the projections for an line of sight (LOS) parallel to the z-axis, i.e. perpendicular to both the nebula axis of symmetry and the external magnetic field, as well as for an LOS tilted by 30°. The gas distribution is overplotted by the magnetic field lines, represented as red tubes. Model BIP9, with $B_0 = 5\ \mu$G, shows magnetic field lines that are distorted by the expanding shell. The field lines lay over the nebula once compressed by the flow, and are stretched into different directions due to the gas motions. Naturally, the nebular axis of symmetry is not aligned to the external magnetic field. For BIP10, on the other hand, the strong external field of $B_0 = 500\ \mu$G is responsible for the break of the nebular expansion towards the direction perpendicular to $\boldsymbol{B}_0$. The shell therefore expands further along the field lines. The final morphology presents itself aligned to the external field.

Note that even in the strongly magnetized case the ambient field lines are perturbed at the shell surface. Naturally, this perturbation will propagate outwards, as explained before, as magnetosonic and Aflvén wave modes. The excitement of such modes is the result of the energy transfer from the expanding shell to the ambient field. An important issue on this process is that polarization vectors may not

trace the original orientation of the external field but would rather represent the local orientation of the perturbed components as well. Considering that magnetic fields would be responsible for most of the dust alignment in evolved PNe, we calculate the synthetic polarization distributions for both models as follows.

3.3 Dust polarization

The effects of external magnetic fields in shaping the PNe at the centre of the Galaxy could possibly be probed by means of polarization maps. Polarization by dust is one of the mechanisms known and it has been extensively applied on the mapping of magnetic fields in many astrophysical environments. Polarization by dust may occur from dust intrinsic emission as well as dust absorption of background radiation. The typical small column densities of the dust component in PNe, compared to that of the ISM, makes the detection of local polarization from PNe and proto-PNe challenging. Even though, these have been reported in some PNe and proto-PNe (e.g. Scarrott & Scarrott 1995; Jurgenson et al. 2003; Su et al. 2003; Ueta, Murakawa & Meixner 2007). Sabin, Zijlstra & Greaves (2007) also reported polarization measurements from infrared emission of dust grains. Different processes may lead to grain alignment, such as a strong radiation source or magnetic fields. It is interesting then to determine how polarization maps, if observed, would trace the relationship between the morphology of the expanding nebula and the external interstellar fields. Here, we consider the magnetic alignment process only, and neglect the radiation pressure from the CS. This assumption is plausible at evolved stages of PNe, though the radiative alignment may be dominant at the early proto-PN phases. The physics of grain alignment with ambient magnetic fields is a complex subject and is not in the scope of this study, therefore, we will perform a simplified calculation of the polarization.

For each cell of the simulated cube, the angle of alignment (ψ) is determined by the local magnetic field projected into the plane of sky, and the linear polarization Stokes parameters q and u are then given by

$$q = \epsilon\rho \cos 2\psi \sin^2 i,$$

$$u = \epsilon\rho \sin 2\psi \sin^2 i, \qquad (16)$$

where ρ is the local density and i is the inclination of the local magnetic field with respect to the line of sight. The 'observed' values of Q and U are obtained by integrating q and u along the LOS, respectively. The polarization degree is obtained as $p = \sqrt{Q^2 + U^2}/I$ and the polarization angle by $\phi = \frac{1}{2}\arctan(U/Q)$.

In Fig. 6, we present the synthetic polarization maps of the two models shown in Fig. 5. The maps represent the emission measure overplotted by the polarization vectors expected to be observed in such systems.[2] We assumed a homogeneous dust alignment efficiency along the whole nebula.

As mentioned before, based on the 3D visualization of the nebulae, the polarization vectors for $B_0 = 500\,\mu$G (top) are not uniform – as could be previously thought – but are also changed by the dynamics of the nebula. This is because the magnetic field probed by the dust polarization is actually the field within the nebular material, i.e. which has already interacted with the ejecta. At the edges of the nebula, the polarization vectors follow the density

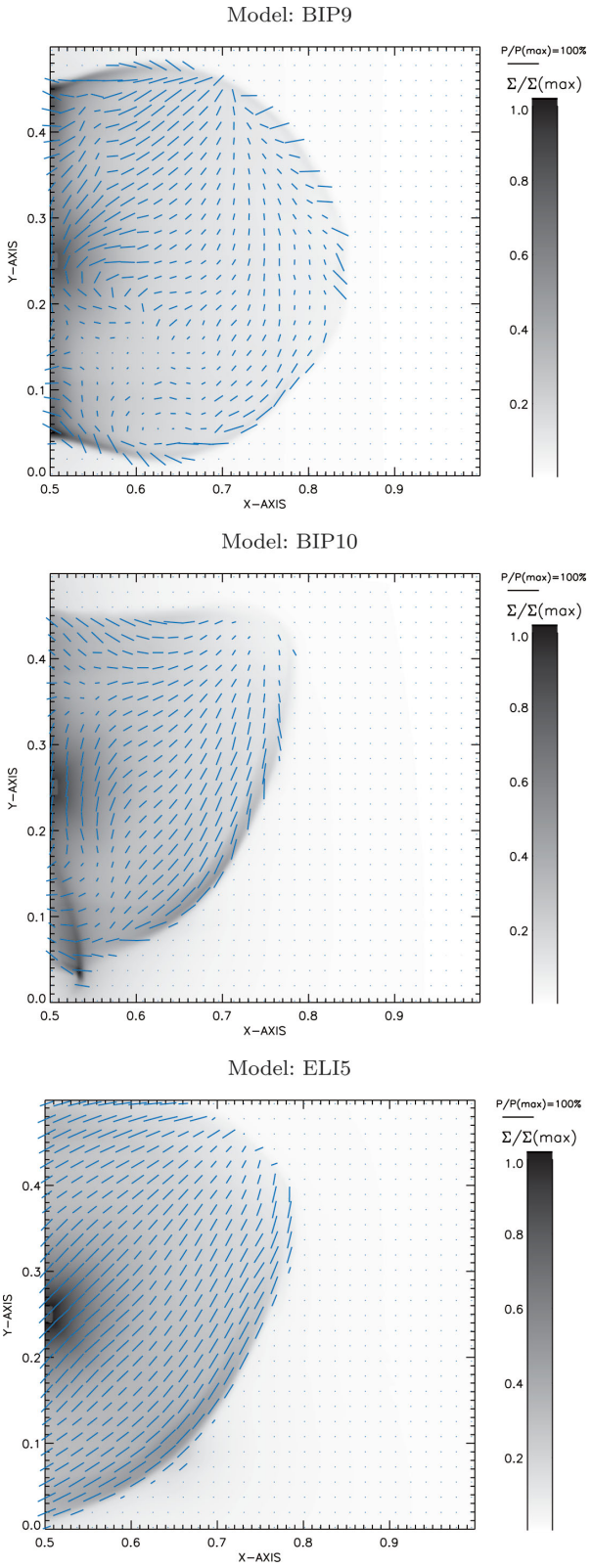

Figure 6. Synthetic polarization maps obtained for the models with $\alpha = 0.95$ (bipolar), being $B_0 = 5\,\mu$G (top) and $B_0 = 0.5$ mG (middle). The bottom image represents the polarization map for model with $\alpha = 0.6$ (elliptical) and $B_0 = 0.5$ mG.

[2] Note that here we consider the polarized dust infrared emission and therefore the polarization vectors have been rotated by 90°. If one considers the dust absorption of background radiation, the polarization will present a change in relative amplitude and the rotation is not needed.

contours. For $B_0 = 5\,\mu$G (bottom), we obtain a more complex distribution of the polarization vectors. It is also noticeable that the polarization intensity is more uniform in the strongly magnetized case compared to the synthetic map for $B_0 = 5\,\mu$G. The main reason for the variation in polarization degree is the local non-uniformity of the field lines as these are integrated along the line of sight, which is larger for the weak magnetic field case.

4 DISCUSSION AND CONCLUSIONS

In this work, we studied the dynamical effects of interstellar magnetic fields on the morphology of PNe. We focus on the late stages of the nebulae expansion, as we assume that the origin of the intrinsic morphology of the PNe is unrelated to the large-scale interstellar properties.

In a very simplified analytical approach, it is possible to understand the magnetic pressure at the shell surface as the nebulae expand over the ISM. It is possible to estimate that a PN would have its morphology modified by the external field once its ram pressure becomes equivalent to the total piled-up field. This picture is different from that of models that consider a static ambient field. For a typical PN, this occurs at $t < 10^4$ yr for an ambient field of $B_0 > 100\,\mu$G. Naturally, this is way too strong magnetic field compared to the estimates of the ISM magnetic field in the solar neighbourhood and in most regions of the Galactic plane ($\sim 2-5\,\mu$G) (see Beck 2009, for a review). An exception to that is the Galactic centre/inner bulge. The study of the magnetic field at the central regions of the Galaxy is challenging, specially at the disc plane due to sources of contamination and absorption.

Polarization of radio continuum from the central few hundreds of parsecs reveal a dominantly poloidal magnetic field, i.e. perpendicular to the disc plane. Magnetic field intensities of 100–1000 μG (see Yusef-Zadeh, Wardle & Parastaran 1997; Chuss et al. 2003; Noutsos 2012) had been inferred. Lower limits of $>50\,\mu$G have also been determined from γ-rays (Crocker et al. 2010) for those regions. The poloidal component is possibly associated with a galactic wind, possibly driven by the strong stellar feedback at the central regions of the Milky Way. These winds would drag the field lines to the observed configuration. The situation is reversed at the disc plane. The ISM rotating around the Galactic Centre would on the other hand keep a dominantly toroidal component, possibly of the same order of magnitude. This idea has been corroborated by recent studies that reveal a toroidal large-scale field with intensities of mG (Ferrière 2009; Nishiyama et al. 2010). Therefore, the current understanding is that of a two-component magnetic field, being one toroidal (mostly at the disc plane) and another poloidal, perpendicular to the disc, mostly permeating the large height parts of the bulge and the inner halo.

The detection of such strong fields reveals the importance of taking into account the interstellar magnetism on (re)shaping Galactic PNe. Despite its low relevance for most of the Galactic disc, the magnetic fields would distort (or bend) nebulae located at the central regions. This can explain the divergent conclusions of Corradi et al. (1998) with those of Melnick & Harwit (1975); Phillips (1997); Weidmann & Díaz (2008) regarding the alignment of PNe with respect to the galactic disc. Also, it is in agreement with the recent work of Rees & Zijlstra (2013) that showed statistically significant alignment of bipolar PNe at the central region of the Galaxy. This also leads to the conclusion that the magnetic fields are possibly the dominant agent on the PNe alignment process, and the eventual alignment of the PN with the disc plane is just the consequence of a magnetic field lying parallel to the disc plane. We could also suggest that the correlation between the alignment of PNe with respect to the disc plane to be a function of the Galactic latitude, even at the Galactic centre. This is because the dominant component transits from toroidal to poloidal with increasing height with respect to the disc plane. However, it is difficult to predict at what heights the PNe would change from toroidal to poloidally aligned, mostly because of the large uncertainties on the observational estimates of $\boldsymbol{B}$.

Our analytical estimates were confirmed by a series of numerical simulations. We performed a number of 2.5- and 3-dimensional MHD simulations in order to verify the validity of the simplified analytical model. We assume the anisotropic preset density distribution as the original shaping mechanism of the nebula. Previous numerical simulations have already tested similar systems (see e.g. Heiligman 1980; Stone & Norman 1992; Matt et al. 2006), but focused on the original shaping of the nebula, or assumed parallel symmetries with respect to the ambient field. Here, the models were run with tilted external magnetic fields, with respect to the original axis of symmetry of the PN, aiming to study the distortion of evolved PNe by external fields.

We found that typical ISM fields of few μG are unable to change the dynamics of the ejecta. Also, even strong fields are unable to modify the shape of the nebulae (e.g. to transform a round nebula into a bipolar one). However, we show that strong magnetic fields are able to tilt the axis of symmetry of originally aspherical PNe. The alignment of the nebula axis of symmetry with respect to the large-scale external magnetic field. This process is more pronounced in bipolar nebulae, compared to the other morphologies. This finding is in particular agreement with the findings of Rees & Zijlstra (2013), which showed a preferential alignment for bipolar nebulae as well.

These results are in agreement with Grinin & Zvereva (1968) and, since $\boldsymbol{B}$ is toroidal at low Galactic latitudes, i.e. the field lies on the Galactic plane, they are also in agreement with Melnick & Harwit (1975); Phillips (1997); Weidmann & Díaz (2008); Rees & Zijlstra (2013). At larger Galactic radii and at high latitudes $\boldsymbol{B}$ is either weak or unrelated to the Galactic plane, therefore, we consider that our results also agree with Corradi et al. (1998). We found good correspondence with the analytical estimates: (i) for the minimum magnetic field intensity required to dynamically affect the expansion of a typical nebula, as $B_0 > 100\,\mu$G and (ii) found the geometry of the magnetic fields at the PNe to be non-uniform, despite of the previous models that assumed static field lines.

One could imagine that polarization maps of planetary nebulae would be useful in probing the orientation and intensity of the interstellar field, due to its imprint on the polarization vectors of the nebula lobes. To investigate this, we calculated synthetic polarization maps from the 3D MHD models. The maps showed no preferential alignment, except for a slightly larger polarization degree along the direction parallel to the external field. Also a small uniformity of polarization vectors is seen in that direction. The complexity of the polarization maps, even in the strongly magnetized case, is related to the fact that the magnetic energy is concentrated right outside the dense nebula. The motions in the shell are actually super-Alfvénic and the field lines will be distorted in any case. Since most of the polarization is due to the denser regions, the intense magnetic field is not probed.

Our results also show that Galactic PNe could be aligned to the Galactic plane, if the local field is parallel to the Galactic disc and if its intensity is large ($>100\,\mu$G). The reason for the alignment is simply the dynamical effect of the magnetic pressure in modifying the expansion velocities of the ejecta.

Finally, our model predicts that the alignment correlation should be size/age dependant. If the angular momentum of the progenitor

star is unrelated to the external field, the initial orientation of the PNe should be random. Only after expanding to quasi-equipartition with the ISM magnetic pressure, the nebula would be tilted. From our estimates, this should occur around $\sim 10^3$ yr after ejection. If we consider a typical expansion velocity of few tens of km s^{-1}, we obtain angular lobe lengths of $l < 0.5$ arcsec for objects at the central region of the Galaxy. Unfortunately, the data of Rees & Zijlstra (2013) is dominated by objects larger than 1 arcsec, and this prediction could not be tested. It would be interesting for future observational surveys with high spatial resolution to explore this prediction.

ACKNOWLEDGEMENTS

DFG thanks the European Research Council (ADG-2011 ECOGAL), and Brazilian agencies CNPq (no. 300382/2008-1), CAPES (3400-13-1) and FAPESP (no.2011/12909-8) for financial support. HM thanks CNPq grant 573648/2008-5 and FAPEMIG grants APQ-02030-10 and CEX-PPM-00235-12.

REFERENCES

Ali A., Sabin L., Snaid S., Basurah H. M., 2012, A&A, 541, 98
Balick B., 1987, AJ, 94, 671
Balick B., Frank A., 2002, ARA&A, 40, 439
Balick B., Preston H., 1987, AJ, 94, 958
Balick B., Preston H., Icke V., 1987, AJ, 94, 1641
Balick B., Owen R., Bignell C. R., Hjellming R. M., 1997, AJ, 94, 948
Beck R., 2009, Astrophys. Space Sci. Trans., 5, 43
Blackman E. G., 2008, in Strassmeier K. G., Kosovichev A. G., Beckman J. E., eds, Proc. IAU Symp. Vol. 259, Cosmic Magnetic Fields: From Planets, to Stars and Galaxies. Cambridge Univ. Press, Cambridge, p. 35
Chuss D. T., Davidson J. A., Dotson J. L., Dowell C. D., Hildebrand R. H., Novak G., Vaillancourt J. E., 2003, ApJ, 599, 1116
Corradi R. L. M., Aznar R., Mampaso A., 1998, MNRAS, 297, 617
Crocker R. M., Jones D. I., Melia F., Ott J., Protheroe R. J., 2010, Nature, 463, 65
Curtis H. D., 1918, Publ. Lick Obs. 13, 57
Dedner A., Kemm F., Kröner D., Munz C.-D., Schnitzer T., Wesenberg M., 2002, J. Comput. Phys., 175, 645
Falceta-Gonçalves D., Jatenco-Pereira V., 2002, ApJ, 576, 976
Falceta-Gonçalves D., Lazarian A., 2011, ApJ, 735, 99
Falceta-Gonçalves D., Vidotto A., Jatenco-Pereira V., 2006, MNRAS, 368, 1145
Falceta-Gonçalves D., de Gouveia Dal Pino E. M., Gallagher J. S., Lazarian A., 2010a, ApJ, 708, L57
Falceta-Gonçalves D., Caproni A., Abraham Z., Teixeira D. M., de Gouveia Dal Pino E. M., 2010b, ApJ, 713, L74
Falceta-Gonçalves D., Lazarian A., Houde M., 2010c, ApJ, 713, 1376
Ferrière K., 2009, A&A, 505, 1183
García-Segura G., 1997, ApJ, 489, L189
García-Segura G., Langer N., Rozyczka M., Franco J., 1999, ApJ, 517, 767
Gnat O., Sternberg A., 2007, ApJ, 168, 213
Grinin V. P., Zvereva A. M., 1968, in Osterbrock D. E., O'Dell C. R., eds, Proc. IAU Symp. Vol. 34, Planetary Nebulae. Reidel, Dordrecht, p. 278
Gurzadyan G. A., 1969, Planetary Nebulae. Gordon and Breach, New York
He Z., Li X., Fu D., Ma Y., 2011, Sci. China Phys., Mech. Astron., 54, 511
Heiligman G. M., 1980, MNRAS, 191, 761
Icke V., Preston H. L., Balick B., 1989, AJ, 97, 462
Icke V., Balick B., Frank A., 1992, A&A, 253, 224
Jurgenson C. A., Stencel R. E., Theil D. S., Klebe D. I., Ueta T., 2003, ApJ, 582, L35
Kahn F. D., West K. A., 1985, MNRAS, 212, 837
Khromov G. S., Kohoutek L., 1968, in Osterbrock D. E., O'Dell R., eds, Proc. IAU Symp. Vol. 34, Planetary Nebulae. Dordrecht, Reidel, p. 227
Kowal G., Lazarian A., 2010, ApJ, 720, 742
Kowal G., Falceta-Gonçalves D. A., Lazarian A., 2011a, New J. Phys., 13, 3001
Kowal G., de Gouveia Dal Pino E. M., Lazarian A., 2011b, ApJ, 735, 102
Kowal G., de Gouveia Dal Pino E. M., Lazarian A., 2012, Phys. Rev. Lett., 108, 241102
Leão M. R. M., de Gouveia Dal Pino E. M., Falceta-Gonçalves D., Melioli C., Geraissate F. G., 2009, MNRAS, 394, 157
Manchado A., 2004, in Margaret M., Joel H. K., Bruce B., Noam S., eds, ASP Conf. Ser. Vol. 313, Asymmetrical Planetary Nebulae III: Winds, Structure and the Thunderbird. Astron. Soc. Pac., San Francisco, p. 3
Masson C. R., 1990, ApJ 348, 580
Matt S., Frank A., Blackman E. G., 2006, ApJ, 647, 45
Melioli C., de Gouveia Dal Pino E. M., de La Reza R., Raga A., 2006, MNRAS, 373, 811
Mellema G., Eulderink F., Icke V., 1991, A&A, 252, 718
Melnick G., Harwit M., 1975, MNRAS, 171, 441
Mignone A., Bodo G., 2006, MNRAS, 368, 1040
Monteiro H., Falceta-Gonçalves D., 2011, ApJ, 738, 174
Nishiyama S. et al., 2010, ApJ, 722, L23
Noutsos A., 2012, Space Sci. Rev., 166, 307
Pascoli G., 1985, A&A, 147, 257
Phillips J. P., 1997, A&A, 325, 755
Poidevin F., Falceta-Gonçalves D., Kowal G., de Gouveia Dal Pino E., Magalhaes A. M., 2013, ApJ, 777, 112
Ransom R. R., Uyaniker B., Kothes R., Landecker T. L., 2008, ApJ, 684, 1009
Rees B., Zijlstra A. A., 2013, MNRAS, 435, 975
Ruiz L. O., Falceta-Gonçalves D., Lanfranchi G. A., Caproni A., 2013, MNRAS, 429, 1437
Ruuth S. J., 2006, Math. Comput., 75, 183
Sabin L., Zijlstra A. A., Greaves J. S., 2007, MNRAS, 376, 378
Scarrott S. M., Scarrott R. M. J., 1995, MNRAS, 277, 277
Schwarz H. E., 1994, in Clegg R. E. S., Stevens I. R., Meikle W. P. S., eds, Proc. 34th Herstnonceux Conf. Cambridge, Circunstellar Media in the Late Stages of Stellar Evolution. Cambridge Univ. Press, Cambridge, p. 274
Shaw R. A., 2012, in Manchado A., Stanghellini L., Schönberner D., eds, Proc. IAU Symp., Vol. 283, Planetary Nebulae: An Eye to the Future. Cambridge Univ. Press, Cambridge, p. 156
Smith H., 1976, MNRAS, 175, 419
Soker N., Dgani R., 1997, ApJ, 484, 277
Stanghellini L., 1999, in Kastner J. H., Soker N., Rappaport S., eds, ASP Conf. Ser. Vol. 199, Asymmetrical Planetary Nebulae II: From Origin to Microstructures. Astron. Soc. Pac., San Francisco, p. 441
Stone J. M., Norman M., 1992, ApJ, 389, 297
Su K. Y. L., Hrivnak B. J., Kwok S., Sahai R., 2003, AJ, 126, 848
Taylor G., 1950, Proc. R. Soc. A, 201, 159
Ueta T., Murakawa K., Meixner M., 2007, AJ, 133, 1345
Van Winckel H., 2003, ARA&A, 41, 391
Vidotto A., Falceta-Gonçalves D., Jatenco-Pereira V., 2006, Space Sci. Rev., 122, 181
Wareing C. J., Zijlstra A. A., O'Brien T. J., 2007, MNRAS 382, 1233
Weaver R., McCray R., Castor J., Shapiro P., Moore R., 1977, ApJ, 218, 377
Weidmann W. A., Díaz R., 2008, PASP, 120, 380
Woltjer L., 1972, ARA&A, 10, 129
Wu Z-Y., Ma J., Zhou X., Du C-H., 2001, AJ, 141, 104
Yusef-Zadeh F., Wardle M., Parastaran P., 1997, ApJ, 475, L119
Zhang C. Y., Kwok S., 1998, ApJ, 117, 341

This paper has been typeset from a TEX/LATEX file prepared by the author.